Performance and liquid water distribution in PEFCs with different anisotropic fiber directions of the GDL

Kyaw Swar Soe Naing*, Yutaka TABE, Takemi CHIKAHISA

Division of Energy and Environmental Systems, Graduate School of Engineering,

Hokkaido University

N13 W8, Kita-ku, Sapporo 060-8628, Japan

* Corresponding author. Tel.: +81 11 706 6333; fax: +81 11 706 7889.

E-mail address: kssn@eng.hokudai.ac.jp; N13 W8, Kita-ku, Sapporo 060-8628, Japan

Abstract

To maintain the efficiency of proton exchange membrane fuel cells (PEFC) without flooding, it is necessary to control the liquid water transport in the gas diffusion layer (GDL). This experimental study investigates the effects of the GDL fiber direction on the cell performance using an anisotropic GDL. The results of the experiments show that the efficiency of the cell is better when the fiber direction is perpendicular to the channel direction, and that the cells with perpendicular fibers are more tolerant to flooding than cells with fibers parallel to the channel direction. To determine the mechanism of the fiber direction effects, the liquid water behavior in the channels was observed through a glass window on the cathode side. The observations substantiate that the liquid water produced under the ribs is removed more smoothly with the perpendicular fiber direction. Additionally, the water inside the GDL was frozen to observe its distribution using a specially made cell broken into two pieces. The

photographic results show that the amount of water under the ribs is larger than that under the channels using the parallel fiber direction GDL while the water distributions in these two places are almost equal level with the perpendicular fiber direction GDL. This freezing method confirmed the better liquid water removal ability and better reactant gas transportation in the GDL with the fiber direction perpendicular to the channel direction.

Keywords: PEM fuel cell, Gas diffusion layer, Anisotropic fiber direction, Visualization, Freezing method

1. Introduction

Improvements in water management are necessary to increase the power densities of PEM fuel cells. The gas diffusion layer (GDL) of PEM fuel cells has to supply reactant gases to the catalyst layer (CL) and remove the produced water from the catalyst layer, and here the GDL plays a crucial role in the water management and is important to mitigate water flooding phenomena. A variety of experimental studies have been carried out to investigate the effects of the GDL thickness, porosity, permeability, and wettability on the performance of PEM fuel cells [1-5]. However, there has been little investigation on the effects of the in-plane carbon fiber directions of the GDL. Commonly-used GDLs have in-plane isotropy and random carbon fiber directions while anisotropic GDLs have partially specifically oriented fiber directions as shown in Fig. 1. The main objective of the paper here is an experimental investigation of the effects of the carbon fiber directions on the cell performance.

A number of experimental methods for investigations of liquid water behavior inside the GDL of PEM fuel cells have been reported, as well as many in-situ visualization methods were reported including neutron radiography/tomography [6], X-ray micro tomography [7], and direct imaging/visualization [8, 9]. Although neutron imaging and X-ray imaging techniques were developed for in-situ visualization and even when they can detect the water inside GDL, these techniques suffer from limited spatial and temporal resolution. Tabe et al. reported the liquid water behavior in PEM fuel cells and described the unique mechanisms in the gas flow in GDLs using direct visualization methods [8]. The report showed that the direct visualization method can provide information with high temporal and spatial resolution to investigate water transport phenomena in the gas flow channels and upper layers of the GDL. Further, we have been unable to locate reports of experiments investigating fuel cells with anisotropic GDL. Guangli et al. investigated only the effects of thermal conductivity of anisotropic GDL but the water distribution inside the GDL affected by the anisotropic GDL was not discussed [10].

In this study, the cell performance with anisotropic GDL of different orientations were measured to investigate the effects of the carbon fiber direction, and the visualization of the water distributions in the channels and GDL were used to clarify the causes of the anisotropic effects of the GDL. The commonly-used direct observations through a window allows visualization of liquid water behavior only in the gas flow channels, and a new method involving freezing of the water in the cell is proposed and used as an ex-situ method to investigate the water distribution inside the GDL. In this freezing method, a small cell was modified so the bipolar plates can be separated into two parts. The liquid water produced

inside the cell was frozen, and then the ice distribution in the cross-sectional view of the cell was investigated by cutting the cell at the boundary between the two pieces. A similar method was applied to investigate the ice distribution at cold starting where the ice is not inside the GDL but on the surface of the MEA and the GDL [11, 12].

2. Experimental apparatus and methods

2.1 Cell for direct observation of liquid water in channels

Fuel cell tests of the performance and direct observations of the channels were conducted with a 25 cm^2 active area cell as shown in Fig. 2. The cathode separators have open channels through which the GDL surfaces can be observed, and this cell can be used to capture the liquid water flow inside the flow channel of the cell from the window of the cathode side by a CCD camera. Separators with straight or serpentine channels were used on the cathode side, and a separator with straight channels was used on the anode side. The width of the channels and land areas of the cathode separators were 2.0 mm. The separators were gold coated copper plate-separators, and the thickness of the separators, which corresponds to the height of the channels, was 0.5 mm. The width of the channels and land areas of the anode separators were 1.0 mm and the height was 0.6 mm. The MEA was PRIMEA (Japan GORE-TEX Inc.). Generally, commonly-used GDLs have random and isotropic carbon fiber directions. However, the GDL used in this investigation has partially oriented fiber directions as explained in the previous section. The structural properties of anisotropic GDL are

summarized in Table 1. The upper one of Fig. 1 shows the surface of anisotropic GDL and the red arrow line indicates the general fiber orientation. Comparing the picture of the anisotropic GDL with the picture of isotropic GDL, the difference in the fiber orientation in the two GDL's is apparently seen in the figure. The ratio of the gas permeability in two different directions is 1.6 as shown in Table 1, showing the degree of anisotropy of the GDL. In the following, one configuration is termed "perpendicular", where the averaged fiber direction is perpendicular to the gas channel direction; and the other configuration is termed "parallel", where the averaged fiber direction is parallel to the gas channels as shown in Fig. 3. The GDLs have the micro porous layer (MPL) at the side of the membrane electrode assembly (MEA). The cell was bound and compressed uniformly by 16.0 mm thick end plates. The cell resistance was measured by an alternating impedance meter at 1.0 kHz, and the cell voltage, impedance, and pressure drop in the gas flow were recorded on a computer at 1.0 second intervals.

In the experiments, the cell was set vertically as in Fig. 2, and the cell temperature was controlled by an electric heater on the anode end plate. For both the parallel and perpendicular cells, the experiments were conducted with pure hydrogen as the anode gas, and pure oxygen or air as the cathode gas. Before the experiments, the overall cell resistance was set to a same value for both cells. Using two types of cathode separators, serpentine and straight, experiments were conducted to measure the voltages at various current densities for the two fiber directions of the GDL. The effects of gas flow rates, humidity conditions, and oxygen concentrations were also analyzed to examine the effects of the carbon fiber direction. The liquid water production behavior on the surface of the GDL was observed through the open

channels of the metal separator as shown in Fig. 2. For this observation, the serpentine separator which has the features of effective water removal and a reasonable pressure drop [13, 14] was used.

2.2 Cell for cross section observation inside GDL

The extensive ex-situ study of the liquid water distributions in the anisotropic GDL was conducted with an especially made cell. This cell allows observation of details of the water behaviors inside the GDL by freezing the accumulated water and visualizing the cross-sectional GDL. During freezing, the GDLs may be deformed when they are separated from the bipolar plates because they adhere firmly with the ice. To avoid the GDL deformation, the bipolar plates consist of two separate sections for each side as shown in Fig. 4. The space between the two pieces was filled by silicon sheet matching the cross section of the bipolar plate channels. The cell has gold coated copper plate-separators with straight channels, and the current was transmitted through the ribs of the flow fields to the collectors.

At the start of the experiment, the cell was operated with a high current density, 1.0 A cm^{-2} for 2.0 hours, because the conditions at the high current density were considered to provide better opportunities for the observation of the liquid water inside the GDL. The cell was placed in an incubator to control the cell temperature. Then, the cell was frozen to -0˚C for about 30 minutes in a thermostatic chamber (COSMOPIA; Hitachi). In the frozen state, the cell was disassembled into its parts in this thermostatic chamber. Then, the GDL was cut, still in the thermostatic chamber, with a sharp knife (a scalpel as used in medical applications)

into two pieces at the silicon interface to observe the cross sectional ice distribution, and the observations were performed by a Leica microscope (Z16 APO) in the thermostatic chamber. The cell was cut from the cathode side, to enable the cathode sides of GDL and MEA to be cut with negligible damage or delamination effects. The cutting paid attention to the need to obtain good images of the frozen water because the sectioning itself may cause delamination [12]. Image processing was conducted to identify the ice locations by comparing pictures with the frozen water deposits and pictures taken after the ice was evaporated. The developed freezing method was demonstrated to be effective to investigate the water distribution in the cell.

Zhigang et al. have suggested that the water within a fuel cell may possibly redistribute itself and move from region to region after cell operation has been shut down [15]. To investigate the water movement between the time when the operation was stopped and the frozen state, an experiment was conducted with a transparent acrylic cell. In this experiment, no current was generated and the experiment was conducted with only oversaturated (RH 200%) nitrogen gas to flood the cathode side of the cell, here the cell temperature was maintained at 35 °C in the incubator. After the oversaturated nitrogen gas had condensed and flooded in GDL, the flow of the supply gas was stopped and a photo of the cell at the stopped condition was taken. Then the acrylic cell was frozen in the thermostatic chamber and a further photo of the frozen condition was taken. The photos at the two different conditions, the condition when the supply gas was stopped and the frozen state, were compared to investigate the differences in the water distribution. With this experiment, it was possible to determine that the ice location within the cell at the freezing state is quite similar to the liquid water

distribution at the time when operation is stopped. Water distributions at three different positions (cross-sectional GDL and MEA/MPL interface, MPL/acrylic interface, and GDL/rib interface) were investigated.

3. Results and discussion

3.1 Cell performance for different carbon fiber directions of the GDL

The characteristics of the cell performance with the two carbon fiber directions were investigated at various current densities using the 25 cm^2 active area cell with the cathode separators of serpentine and straight channels. Fig. 5 shows the cell voltages for the two fiber directions at different current densities using the two separator types, serpentine and straight channels. Here, air was used as the cathode gas and pure hydrogen as the anode gas. The stoichiometric ratios were 3.0 for the cathode and 2.0 for the anode at 1.0 Acm^{-2}. The humidity of both gases was set to saturation at 60 °C with the cell temperature at 58 °C. The overall cell resistance in both cells was set equal before the cell operation. The results show that the performances of the two cells are very similar at the lower current densities for both separator types. However, the cell voltages of the perpendicular fiber direction are higher than those with the parallel fibers, and the differences in the cell performances become more apparent when the current densities increase. These results allow the conclusion that the perpendicular fiber direction GDL is superior to the cell with parallel fibers. The differences

become clearer when using the straight channel type cell, as the perpendicular fiber direction becomes parallel to the channels at the U-turns of the serpentine separator. It was also confirmed that the perpendicular fiber direction GDL showed less flooding characteristics than the parallel fiber direction GDL.

The effects of the width of rib on the cell performances were investigated by using the straight cathode separator with the smaller rib width, 1.0 mm, with channel width of 2.0 mm. Although the difference was slightly smaller than in Fig. 5, similar result was observed: i.e. the cell voltages of perpendicular fiber direction were higher than those of the parallel direction in high current density region. The difference was confirmed even with the high stoichiometric ratio of 12.0 at 1.0 Acm^{-2} and oxygen operation. This confirms that the benefit of the perpendicular fiber direction still exists with the smaller width rib.

In order to confirm the above effect of anisotropic GDL, similar experiment was conducted with using an isotropic GDL at the same condition in Fig. 5. The results showed that the same cell performance was obtained over the whole current density range when the isotropic GDL was placed in the different directions of 90 degrees. This result indicates that the cell performance can be affected by the carbon fiber direction of anisotropic GDL. The cell performance of the isotropic GDL was slightly higher than the anisotropic GDL of perpendicular fiber direction. This is due to the different properties of the two GDL's, and it does not mean the general inferiority of anisotropic GDL compared to isotropic GDL.

To investigate the tolerance to flooding, the cell temperatures were varied at two different relative humidity conditions. Fig. 6 shows the cell voltage changes using the two anisotropic GDLs, perpendicular and parallel, at different relative humidity conditions. The

cell temperature was set at 50 °C (top panel of Fig. 6) and 42 °C (bottom panel), which corresponds to RH 60 % and 90 % respectively for the saturation temperature of the inlet gas at 40 °C. The stoichiometric ratios of the hydrogen and air were 1.3 and 3.0 at the current density 0.5 Acm^{-2}. The serpentine channel type was used as the cathode separator in this part of the investigation. Current density was increased gradually to 0.5 Acm^{-2} within 300 seconds, and then maintained at 0.5 Acm^{-2}. For both humidity conditions, the cell voltage of the perpendicular GDL cell is higher than that of the parallel GDL throughout the operation here. The pressure drops are very similar for both conditions over the experimental period. This indicates that the amounts of condensed water in the channels of the two cells are similar for the same current density operation. These results confirm that the perpendicular GDL cell is more tolerant to flooding than the parallel cell. The difference of cell voltages between the perpendicular GDL cell and the parallel cell in RH 90% is higher than that in RH 60%. Further, the differences in the performances with the two different fiber directions in Fig. 6 are smaller than those at 0.5 Acm^{-2} in Fig. 5 with the higher humidity condition, 110 %. The difference of cell performances between two different fiber directions were also investigated at lower humidity condition, RH 40%, and the result showed the smaller difference of cell voltages than those at 60% and 90%. These results show that the benefits of the perpendicular cell become more apparent at higher humidity conditions, indicating that the difference appears to be due to the liquid water behavior in GDL.

Transport of the liquid water varies with current density, temperature, gas humidity, type of separator, cathode gas (air or O_2), and gas flow rate. Therefore, the cell performance at various conditions was investigated using the two cathode separators with straight and

serpentine channels. Table 2 is the conditions and results for 19 set of experiments. Fig. 7 presents the results of comparisons of the cell voltages of the perpendicular and parallel cells for the 19 experimental conditions. The ratio of the cell voltage of the perpendicular cell to that of the parallel cell is expressed in the abscissa in the figure. The ordinate is the number of experiments in each range of voltage ratio. The 19 experiments include various experimental conditions; high or low current density operation with air or oxygen as cathode gas. Humidity conditions (60 ~ 90%) were used for all experiments. The perpendicular cell shows a better performance than the parallel cell when the voltage ratio is larger than one. The results demonstrate that the voltages of the perpendicular cell are higher than those of the parallel cell for all the 19 experiments conducted here. There were four experimental data in the voltage ratio greater than 1.4, whose condition corresponds to relatively higher current density operations (0.7 Acm^{-2}) at lower stoichiometric ratios (2.0 to 3.5) of air and higher current density operation (1.0 Acm^{-2}) with air. In the range, $1.0<V_{per}/V_{para}\leq 1.4$, there were15 experiments; their conditions were relatively lower current density (0.5 and 0.7 Acm^{-2}) and higher stoichiometric ratios of air and the conditions at higher current densities (0.7 and 1.0 Acm^{-2}) with oxygen. From these results, it can be concluded that the perpendicular fiber direction GDL has advantages over the parallel fiber direction GDL and that the effects of the carbon fiber direction of the anisotropic GDL are important in the management of the liquid water transportation. Further, it may be concluded that the differences in the performance of the perpendicular and parallel fiber directions are clearly demonstrated in the operation with air as the cathode gas.

To estimate the differences in the oxygen transport resistance with the two different fiber directions of cathode diffusion medium, limiting current measurements were conducted. Fig. 8 shows plots of the limiting current densities as a function of the oxygen concentration of the cathode for the two different fiber directions. The straight channel cell which shows very different performances for the two fiber directions was used as the cathode separator in this comparison. Constant flow rates, corresponding to the stoichiometric ratios of 3.0 for cathode air and 2.0 for anode hydrogen at 1.0 Acm^{-2}, were used. The temperatures were 60 °C for the saturation temperature of the gases and 58 °C for the cell temperature. The maximum percentage of oxygen in the cathode gas was 30 %. The cell voltage decreased from 0.9 V to 0.0 V when increasing the current density from 0.0 Acm^{-2} to 1.4 Acm^{-2} over a time period of 280 seconds. More gradual increase of the current with longer durations produced no changes in the limiting current measurements. These results show that the limiting current densities of the perpendicular GDL cell are higher than those of the parallel cell for all oxygen concentrations. The current densities approach a limiting value with increasing oxygen concentrations. The limiting value for the perpendicular fiber direction cell appears to be above 1.2 Acm^{-2} while that of the parallel cell is less than 1.0 Acm^{-2}. This substantiates that the use of the perpendicular carbon fiber direction allows an adequate oxygen supply, when comparing with the parallel fiber direction cell.

3.2 Liquid water behavior for the different carbon fiber directions with direct visualization

The characteristics of the water removal from the GDL to the flow channel were investigated using with the 25 cm^2 active area cell. The serpentine separator type which has better drainage characteristics for condensed water [13, 14] was used in the analysis. Fig. 9 shows photos of the growth of the liquid water film in the perpendicular cell and of a droplet in the parallel cell. The photos are direct views of the inside of the flow channel, showing the surface of the GDL downstream of the cathode channel. The stoichiometric ratios of the hydrogen and air were 1.3 and 3.0 for 0.5 Acm^{-2}. The saturation temperature for both inlet gases was set at 40 °C, with the cell temperature at 45 °C (RH 77 %). In these experiments, the cell voltage (data not shown) was also higher with the perpendicular direction GDL than with the parallel direction GDL. For both cases, the photos were taken at the same position, downstream in the channel at different times from the start of operation. The photos show that water film flows from the side of the rib to the channel with the perpendicular fiber direction (the left photos Fig. 9). In this cell operation, the water film grows from the side of the rib to the channel as shown in the photo at 27 min from the start of operation. The growth of the water film from the rib towards the channel can be seen in the photos at 29 min and 33 min. Then, this water film flows in the gas flow direction, left to right in Fig.9, in the channel as shown in the photo at 41 min of the perpendicular case. This shows that the accumulated liquid water inside the GDL under the ribs flows to the channels using the fiber direction perpendicular to the channel. However, with the parallel fiber direction (right photos) there was a liquid droplet at the center of the channel as shown in the right side photos in Fig. 9. In these photos of the parallel case, the droplet is first at the center of the channel as shown in the photo at 21 min, and growth of the droplet can be seen in the photos at 22 min and 24 min.

Then, the droplet flows with the direction of the gas flow in the channel as shown in the photo at 25 min of the parallel case. The behavior of the water in these photos indicates that the water under the ribs may accumulate under the ribs when the fiber direction parallel to the channels was used, and this accumulated water may affect the cell performance. The liquid water behavior shown in these photos displays the general situation in all the recorded photos. The observations indicate that the liquid water produced under the ribs was removed more regularly with the perpendicular direction GDL fibers than with the parallel fiber GDL.

From the water behavior in the cathode channel and the changes in the cell voltage, the process of removing the liquid water from the cell may be summarized as illustrated in Fig. 10. In PEM fuel cell operation, the liquid water generated in the cell accumulates inside the GDL and is expelled through the openings between the fibers in the GDL and flows out to the cell channel [9]. The case with fibers perpendicular to the flow direction in Fig. 10 (top image) suggests that the accumulated water under the ribs is able to flow out to the channels because the produced water is able to move along the GDL fiber direction. Therefore, the accumulated water under the ribs can migrate toward the channels as suggested in the photos of the perpendicular case in Fig.9. In the perpendicular case, there is then adequate space in the GDL to allow the supply gas to flow and more oxygen can be transported to the zone under the ribs. This situation produces a larger number of gas paths to the MEA under the rib areas, resulting in the superior performance of the cell with fibers perpendicular to the flow direction. In the case of the parallel fiber direction in Fig. 10 (bottom image), the water under the ribs cannot easily flow out to the channels because the water produced in the GDL generally moves along the GDL fiber direction. Once the produced water accumulates under the ribs, resulting in the

gas paths under the ribs becoming filled with water. The growth in the volume of accumulated water obstructs the supply of reactant gases and as a result the supply of reactant gases to the MEA under the ribs becomes insufficient as suggested by Fig. 10 (bottom image). Because the liquid water accumulated under the ribs only flows out to the channels with difficulty, and as gas paths in the GDL are open only under the channels, liquid droplets grow from the GDL surface around center of the channel as shown in the right side photos for the parallel case in Fig. 9.

3.3 Liquid water distribution inside the GDL by freezing visualization

To further investigate the effects of the carbon fiber directions on the water distribution inside the GDL, an advanced observation method involving freezing of the accumulated water was developed as mentioned in Section 2.2. A small cell with a reaction area of 2 cm^2 was utilized for this freezing experiment. Experiments with a high current density, 1.0 Acm^{-2}, were conducted to investigate the distribution of the produced water inside the cell in more detail. Stoichiometric ratios of 2.9 for pure hydrogen and 4.0 for pure oxygen were used to maintain the cell performance at 1.0 Acm^{-2}. The cell temperatures were 50 °C to 60 °C with the saturation temperatures at 30 °C to 50 °C, to analyze the various water behaviors in four experimental conditions, with two conditions of higher humidities (RH 78 & 95 %) and two of lower humidities (RH 20 & 28 %). From the cell performances observed in these experiments, the higher humidity conditions will be termed ‘stable’ (RH 78 %) and ‘flooded’ (RH 95 %) in the following, and the lower humidity conditions as ‘stable’ (RH 28 %) and

‘dried out’ (RH 20 %). The time durations of the operation were different in the stable conditions (RH 78 % and 28 %) and the performance decreasing conditions, flooded (RH 95 %) and dried out (RH 20 %). The differences in the characteristics of the water behavior in the cell were hypothesized, and based on this the ice distribution in two places: inside the GDL and the at MEA/MPL interface, was particularly pronounced.

Fig. 11 is an example of subtracted cross-sectional images of the cell using the parallel fiber orientation, and this figure explains the determination of the ice distribution inside the GDL. These images are in the stable condition with high humidity (RH 78%) at the cathode side under the channel. The photos were taken at the same position in the cell for two states, frozen and evaporated, after cutting the cell as explained in Section 2.2. The photos at the evaporated state were taken to observe the position of the carbon black and the fibers of the GDL at the cross sectional images after the ice was melted and had evaporated. Then, the photos of the frozen state were compared with the photos of the evaporated state to determine the ice distribution inside the GDL of the photo with the frozen water. To clearly visualize the form of the ice distribution inside the GDL in the pictures with the frozen water the subtracted photo was used.

The procedure for establishing the subtracted photo was as follows. The photo of the evaporated state (image (b) of Fig. 11) was aligned with the photo including the frozen water (image (a) of Fig. 11) using the software Image Pro. 6.3. Then, the aligned photo of the evaporated state was subtracted by the photo including the frozen water. This allows the ice formations inside the GDL to be visualized in the subtracted image, and is shown in image (c) of Fig. 11.

Fig. 12 shows an example of cross-sectional images of the MEA/MPL interface to determine the water distribution behaviors at the MEA/MPL interface. The images (a) and (b) of Fig. 12 are parts (MEA/MPL interface shown with black outline) of the images (a) and (b) of Fig. 11 respectively. After the freezing process of PEM fuel cell, the amount of the produced water at the interface was analyzed by measuring the thickness of the ice at MEA/MPL interface. The ice was not seen in the catalyst layer or in the MPL with this magnification range. With the freezing technique, the produced water residing between MEA and MPL was frozen and the frozen ice attaches firmly to MEA and MPL. As a consequence, the position of the MEA and MPL at the photos taken after evaporation can be distinguished from those at freezing because the MPL has shifted slightly (away or closer) from the MEA after the ice was evaporated. Although this may also have been the situation inside the GDL, it happened mostly at the MEA/MPL interface. Therefore, it was not possible to describe the water behavior at the MEA/MPL interface by the subtracted photos. Because the membrane and MPL can be observed clearly in the photos with the frozen state, these “landmarks” were used as the reference lines to measure the area between the membrane (anode catalyst layer side) and MPL for the frozen state using the software as shown in the image (a) of Fig.12. This area (I) includes the amount of the ice at the MEA/MPL interface and the area of the catalyst layer and membrane (anode catalyst layer side) as shown in the schematic diagram (c) of Fig. 12. Further, the area (II) of the catalyst layer and membrane (anode catalyst layer side) at the evaporated state was measured as shown in the schematic diagram (c) of Fig. 12. By subtracting the area (II) from the measured area (I) at frozen state, the amount of ice distribution at the MEA/MPL interface was determined. With this amount of ice, the average

produced water thickness at the MEA/MPL interface under the channel and rib areas was estimated.

3.3.1 Water behavior in the GDL in the high humidity conditions

The subtracted cross-sectional GDL pictures using the parallel fiber direction for the high humidity conditions (RH 78 & 95 %) are shown in Fig. 13. The parallel fiber direction GDL were utilized to understand the effects of the humidity conditions on the water distribution behaviors because the differences in water behavior at different positions (under the channels and under the ribs) can be seen more clearly using the parallel fiber direction GDL. The ice inside the GDL is shown with white outlines in these subtracted pictures. The top photos are for the areas under the channel and the rib for the stable condition (RH 78%) and the bottom two photos are for the flooded condition (RH 95%). The photos showing the area under the channels and the ribs at the same humidity condition were compared to establish the differences in water behavior. The photos show that the ice volumes under the rib are larger than under the channel for the stable condition (top photos). The measurements of the water area in photos at three locations in two times of experiments showed that about 11% under the channel and 17% under the rib were flooded inside the GDL. These photos indicate that the produced water accumulates under the ribs using the parallel fiber direction GDL. In the flooded condition, the ice volumes under the channel and rib are very similar or occasionally there are in slightly more ice under the ribs (bottom photos). The measurements of the water area in photos at three locations in two times of experiments showed that the

water areas were about 18% under the channel and 19% under the rib. This indicates that the flooded condition may be caused not only because the water accumulates inside the GDL under the ribs but also because of the increase in accumulated water inside the GDL under the channels. During this experiment, this situation of the ice distributions is the general tendency at all the conditions examined here. The pictures confirm that the liquid water accumulate under the ribs because of the effect of the fiber directions as discussed in the parallel case for Fig. 10 in Section 3.2.

Fig. 14 shows the estimated average produced water thicknesses at the MEA/MPL interface under the channel and rib areas in the four humidity conditions using the parallel direction fibers. This water thickness was determined on the cathode side and it suggests the amount of water accumulating at the MEA/MPL interface (Fig. 12). In this Fig. 14, the maximum and minimum water thickness observed here are shown as error bars. Although the variations of the obtained results are large, the average values of the estimated amounts show the tendency in the amount of accumulating water at the MEA/MPL interface. The results show that the ice under the ribs is smaller than that under the channels in the high humidity conditions (RH 78 % and 95 %). These phenomena are caused by the effect of the fiber direction of the GDL and the blockage of the flow of the accumulated water under the ribs as explained in the parallel case of Fig. 10. Further, the effect of the clamping pressure of the rib onto the GDL must be considered for this case because the compression from the ribs can affect the part of the GDL under the ribs. Comparing the water thickness of the high and low humidity conditions, the thicker ice is in the high humidity conditions. It is clear that the relative humidity affects the water amount at the MEA/MPL interface. Under the low

humidity conditions, the water thickness under the channels and the ribs are very similar and show as the same thickness in both conditions, stable and dried out. In the low humidity conditions, only small amounts of liquid water accumulates because of the larger evaporation speed.

3.3.2 Water behavior inside the GDL affected by the fiber direction

In the investigation of the differences of the water behaviors due to the effect of the carbon fiber directions, cross-sectional images showing the ice distribution of the perpendicular and the parallel fiber directions were used. Fig. 15 shows the subtracted cross-sectional GDL photos with the perpendicular fiber direction on the cathode side under the channel (left) and rib (right) for the high humidity stable (RH 78%) condition. The visualization of the ice distribution inside the GDL is like in Section 3.3.1. The photos in Fig. 15 for the perpendicular cell under the channel and the rib were compared with the top photos of Fig. 13 for the parallel cell under the channel and the rib at the same operating condition (RH 78 %) to investigate the effects of the carbon fiber directions on the water distribution inside the GDL. Comparing the ice photos of under the channel, the ice distributions are almost same for the two different fiber directions. The measurements of the water area in photos at three locations in two times of experiment showed that the water areas in the perpendicular case were about 9% under the channel and 7% under the rib. From the measurements of the water area in the perpendicular and parallel cases, it can be confirmed that the less water accumulated in the perpendicular case than in the parallel case. However,

there is more ice inside the GDL under the rib in the parallel case (top photos of Fig. 13) than in the perpendicular case (Fig. 15). Further, it can be seen that the ice distribution under the channel and rib are very similar in the perpendicular case (Fig. 15) while there is more ice under the rib than that under the channel in the parallel case (top photos of Fig. 13). This suggests that the accumulated water can flow out to the channels along the fiber direction in the perpendicular case as explained for the perpendicular case in Fig. 10. The photos under the rib in Fig. 13 and 15 confirm that the carbon fiber direction perpendicular to the channels gives the better water removal characteristics from the region under the ribs than the parallel case.

Fig. 16 shows the estimated average water thickness at MEA/MPL interface (Fig. 12) for the two different fiber directions in the two humidity conditions. The results at the higher humidity (RH 78 %) and the lower humidity (RH 28 %) conditions were used here. In the low humidity condition, the thickness of the ice under the channels and ribs are almost the same for each cells, and the amounts of the ice distribution are slightly different for the two different fiber orientations. The operation with the lower humidity condition generates less water at the MEA/MPL interface due to the less saturated vapor, and the carbon fiber direction of the GDL does not affect on the water distribution inside the GDL in the low humidity condition.

For the high humidity condition, the thickness of the ice in the perpendicular case is a little larger than in the parallel case. Although the thickness of the ice under the channels is almost the same for the two fiber directions, the thickness is different under the ribs. This could be because the accumulated water hinders the supply of reactant in the parallel case, and thus the amount of produced water from the reaction under the ribs in the parallel case is

lower than that in the perpendicular case. This supports the previous explanations that the reaction rate is lower under the ribs in the parallel case. The results also indicate that more water may be produced under the channels than under the ribs in the parallel case, and that the produced water amounts are almost the same as in the perpendicular case. This confirms that more oxygen can be transported from the channels into the zone under the ribs in the perpendicular case with the result that the limiting current density of the perpendicular cell is better than that of the parallel cell.

The above consideration, however, might be affected by the difference of the clamping pressure for the fiber directions. The difference in the clamping pressure between under the channel and under the rib may be larger for the parallel case than that for the perpendicular case, because the fiber is not oriented from under the rib to under the channel in the parallel case. The observation of the compressed structure of the dry GDL showed that the GDL thickness was 225 μm under the channel and 215 μm under the rib in the parallel case, while it was is 223 μm under the channel and 220 μm under the rib in the perpendicular case. This indicates that the space in the GDL under the clamping pressure was slightly different depending on the fiber direction. This may affect the difference in the water content between the two GDL's.

4. Conclusions

The effect of the fiber direction of an anisotropic GDL on the cell performance was experimentally investigated. The results showed that the efficiency of the cell is better with the

fiber direction perpendicular to the gas channels (perpendicular cell), and the cell with perpendicular fibers is more tolerant to flooding than the cell with fibers parallel to the gas channels (parallel cell). Observation of the liquid water on the surface of the GDL suggests that the differences in the performance of the parallel and perpendicular cells are caused by the water transport characteristics in the GDL: that is, the liquid water produced under the ribs appears to be drained more easily from the reaction zone in the case of the perpendicular fiber direction than in the parallel fiber direction. The carbon fiber direction perpendicular to the channels appears to have better water removal characteristics for the regions under the ribs, resulting in the better cell performance.

To better understand the role of the fiber direction in the water removal ability an advanced visualization using water freezing was developed to explore the liquid water behavior in the cell. Here, cross-sectional images of the cell showed that the amount of accumulated water inside the GDL is larger under the ribs than under the channels with the parallel fiber direction GDL, and this indicates the importance of water removal from the rib zones. A comparison of the cross-sectional images of the cells with the two different fiber directions, perpendicular and parallel, confirmed that the liquid water removal ability and reactant gas transportation of the perpendicular fiber direction GDL is superior to that of the cell with the parallel fiber direction.

Acknowledgment

The authors thank Imra Material R&D Co., Ltd. for provision of the anisotropic GDLs with the valuable information.

5. References

[1] Lee HK, Park JH, Kim DY, Lee TH, J. Power Sources 2004; 131:200–6.

[2] Jordan LR, Shukla AK, Behrsing T, Avery NR, Muddle BC, Forsyth M, J. Power Sources 2000; 86:250–4.

[3] Park GG, Sohn YJ, Yang TH, Yoon YG, Lee WY, Kim CS, J. Power Sources 2004;131:182–7.

[4] Lin G, Nguyen TV, J. Electrochem Soc 2005; 152(10): A1942–8.

[5] Williams MV, Kunz HR, Fenton JM, J. Electrochem Soc 2004;151(10):A1617–27.

[6] T. Kim, C.M. Sim, M.H. Kim, Applied Radiation and Isotopes 66 (2008) 593-605.

[7] T. Mukaide, S. Mogi, J. Yamamoto, A. Morita, S. Koji, K. Takada, K. Uesugi, K. Kajiwara, T. Noma, J. Synchrotron Radiation ISSN 0909-0495.

[8] Y. Tabe, K. Kikuta, T. Chikahisa, M. Kozakai, J. Power Sources 193 (2009) 416-424.

[9] X.G. Yang, F.Y. Zhang, A.L. Lubawy, C.Y. Wang, Electrochemical and Solid-State Letters, 7 (11) A408-A411 (2004).

[10] Gaungli H, Yohtaro Y, Abuliti A, J. Power Sources 2010;195:1551–1560.

[11] Y. Tabe, H. Nakamiya, K. Kikuta, T. Chikahisa, F. Kagami, and K. Yoshizawa, Proceedings of 13th International Heat Transfer Conference, [1/1 (CD-ROM) SOL-08], pp. 1-8, 2006.

[12] S. Kim, B.K. Ahn, M.M. Mench, J. Power Sources 179 (2008) 140-146.

[13] K. Jiao, J. Park, X. Li, Applied Energy 87 (2010) 2770-2777.

[14] J. Park, X. Li, J. Power Sources 163 (2007) 853-863.

[15] Z. Qi, H. Tang, Q. Guo, B. Du, J. Power Sources 161 (2006) 864-871.

Fig. 1. Anisotropic and isotropic GDLs.

Fig. 2. Experimental apparatus for visual observations and a schematic illustration of a 25 cm^2 active area PEFC.

Fig. 3. Two types of configuration of the anisotropic GDLs used in this investigation, perpendicular and parallel fiber directions.

Fig. 4. The 2 cm^2 active area PEFC for cross-sectional observations of the GDL and MEA, here the bipolar plates consist of two separate sections.

Fig. 5. Polarization curves for the two orientations of anisotropic GDL, perpendicular and parallel, with two separator types, serpentine and straight.

Fig. 6. Voltage changes for the two types of anisotropic GDL, perpendicular and parallel, at different humidity conditions (0.5 Acm^{-2}).

Fig. 7. The probability number of experiments resulted in the ratio of voltages of the perpendicular cell to those of the parallel cell in the various conditions tested.

Fig. 8. Limiting current densities with various oxygen concentrations for the two types of cell here.

Fig. 9. Photos of the growth and changes in appearance in the liquid water film in the perpendicular cell and the changes in the size and position of a droplet in the parallel cell taken by direct visualization.

Fig. 10. Experimentally suggested images of liquid water distribution and gas flow paths in the GDL: perpendicular fibers (top) and parallel fibers (bottom).

Fig. 11. Cross sectional views of the cell at the same position of the cathode side in (a) the frozen and (b) the evaporated (after water removal) states, and (c) the subtracted cross sectional view of the GDL with the ice distribution indicated (within white line).

Fig. 12. The cross-sectional view of the MEA/MPL interface with (a) the area (within the yellow lines) of the catalyst and membrane including the ice at the frozen state, and (b) the area (within the yellow lines) of the same layers after water evaporation (please ignore the green character "PG" which is created automatically in software, Image Pro.), (c) schematic diagram of the MEA/MPL interface with the reference lines (yellow lines) to measure the areas expressed in (a) and (b).

Fig. 13. The subtracted cross-sectional view of the GDL in the cathode side showing the ice distribution (within the white outlines) for the parallel fiber cell.

Fig. 14. Estimated average thickness of water at MEA/MPL interface in the parallel cells. The maximum and minimum values are shown as the error bars.

Fig. 15. Subtracted cross-sectional view of the cathode side of the cell with the ice distribution (within the white outlines) for the perpendicular fiber cell.

Fig. 16. Estimated average thickness of water distributions at the MEA/MPL interface in the perpendicular and the parallel cells. The maximum and minimum values are shown as the error bars.

Table 1. Structural properties of anisotropic GDL.

Table 2. Conditions and results for 19 set of experiments.

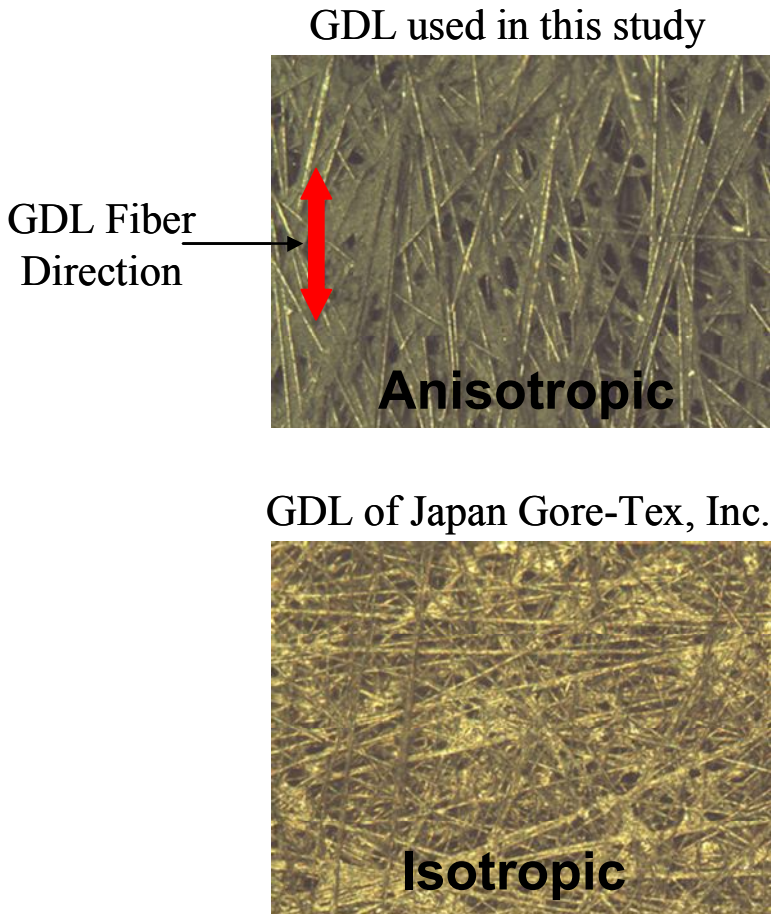
GDL used in this study
GDL Fiber Direction
Anisotropic
GDL of Japan Gore-Tex, Inc.
Isotropic

Fig. 1

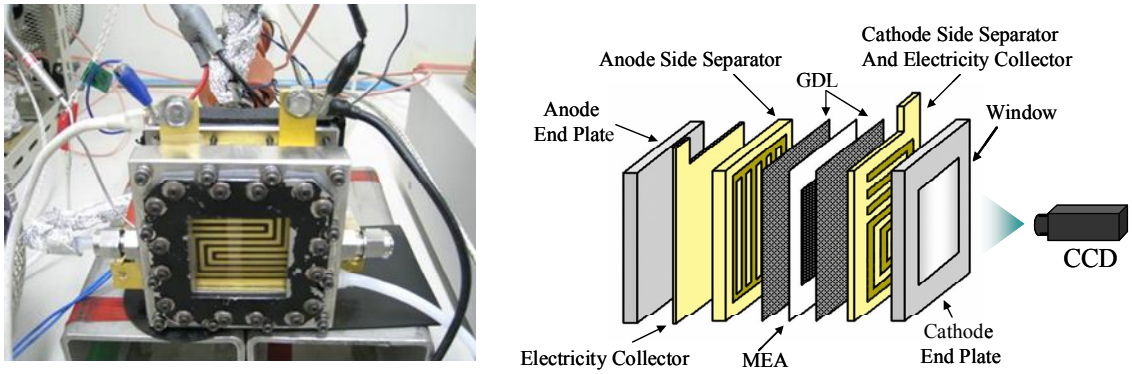
Anode Side Separator
Cathode Side Separator
And Electricity Collector
GDL
Anode
End Plate
Window
CCD
Electricity Collector
MEA
Cathode
End Plate

Fig. 2

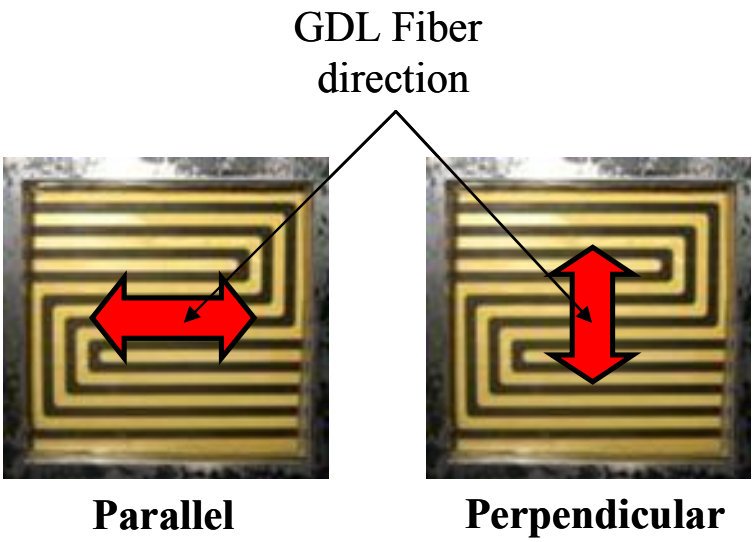

Fig. 3

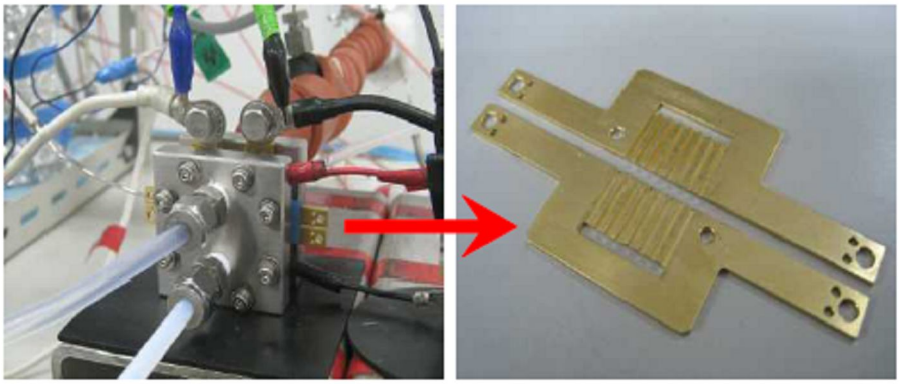

Bipolar plate consists of two separate sections

Fig. 4

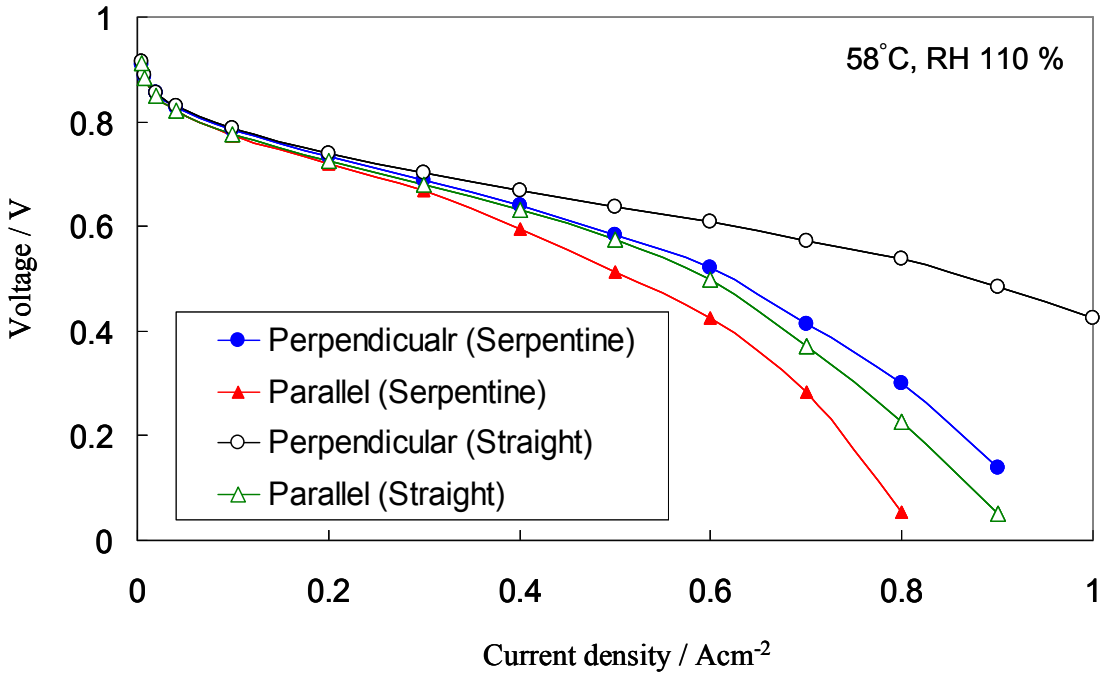
58°C, RH 110 %
Voltage / V
Current density / Acm-2
Perpendicualr (Serpentine)
Parallel (Serpentine)
Perpendicular (Straight)
Parallel (Straight)
0
0.2
0.4
0.6
0.8
1

Fig. 5

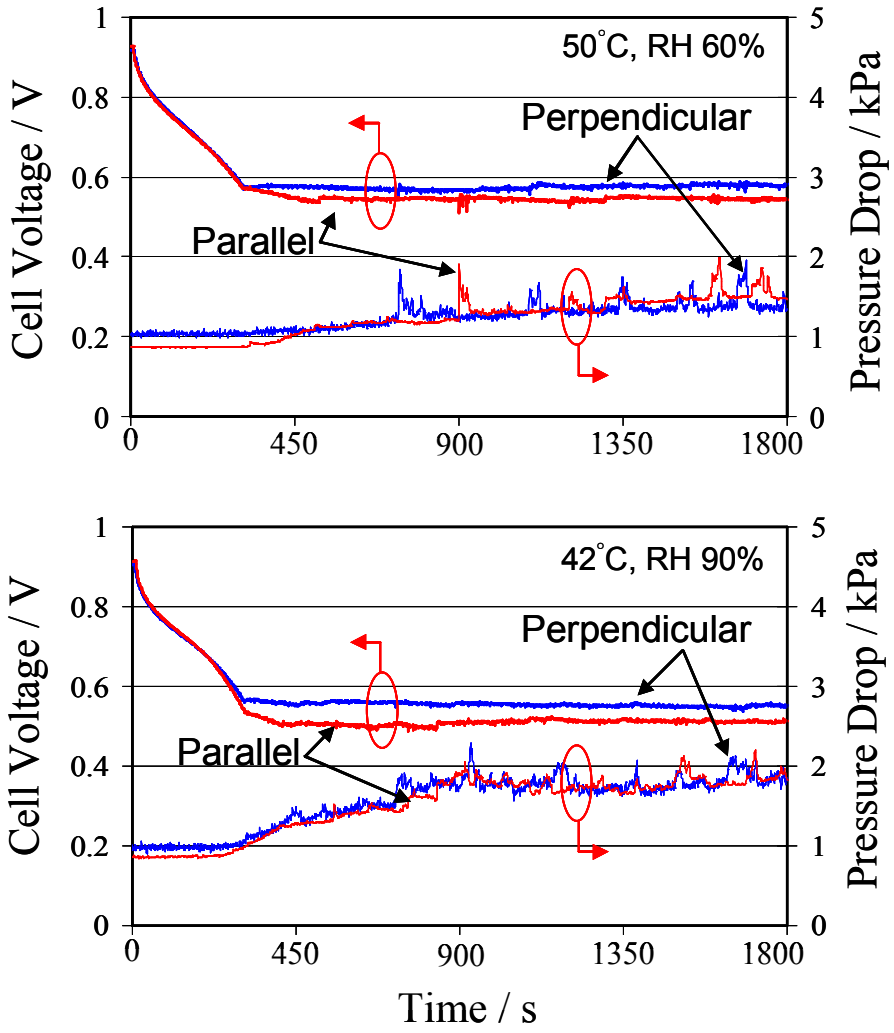
50°C, RH 60%
Perpendicular
Parallel
Cell Voltage / V
Pressure Drop / kPa
42°C, RH 90%
Perpendicular
Parallel
Cell Voltage / V
Pressure Drop / kPa
Time / s

Fig. 6

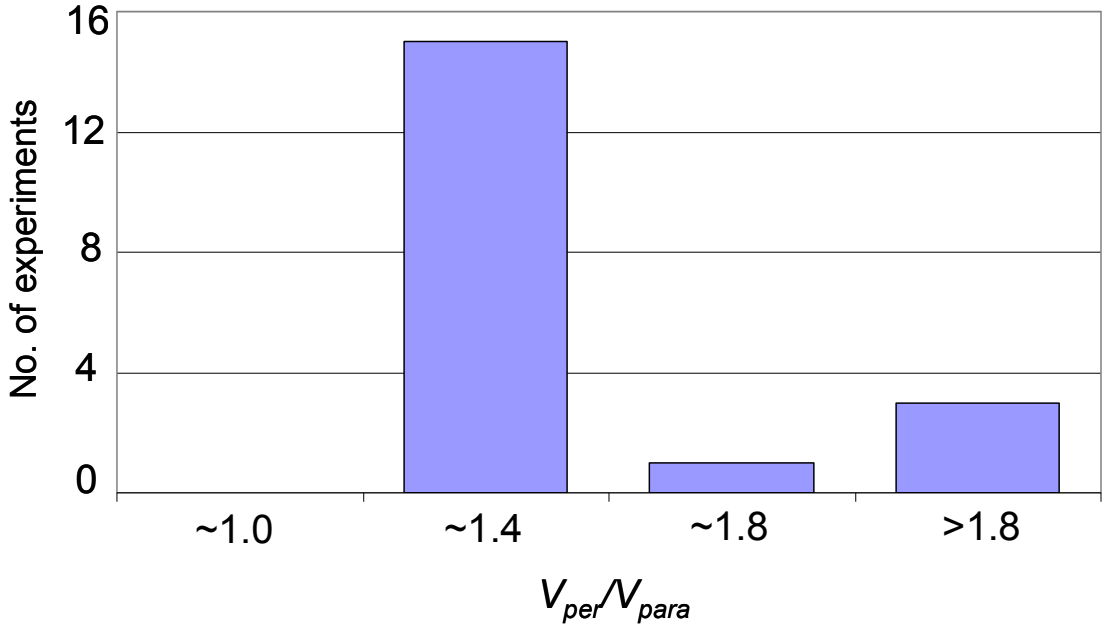

Fig. 7

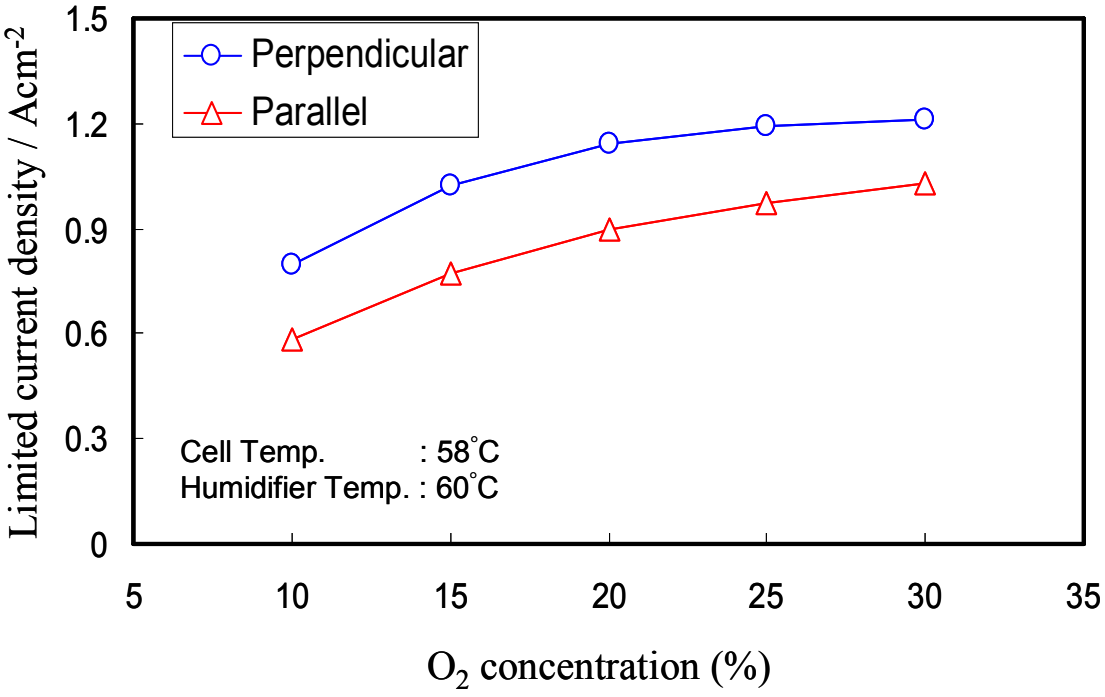
Perpendicular
Parallel
Cell Temp. : 58˚C
Humidifier Temp. : 60˚C
Limited current density / Acm-2
O2 concentration (%)
1.5
1.2
0.9
0.6
0.3
0
5
10
15
20
25
30
35

Fig. 8

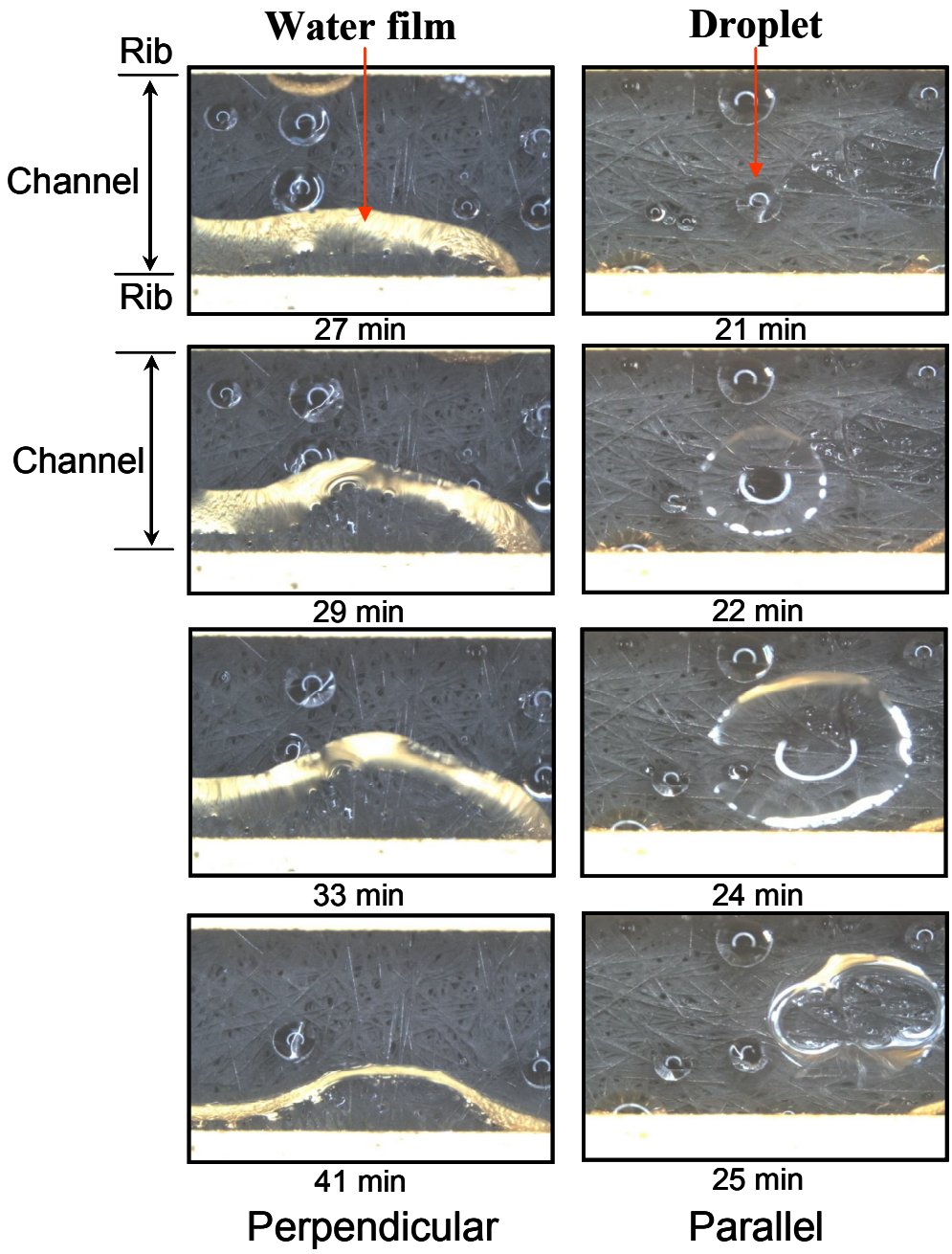
Water film
Droplet
Rib
Channel
Rib
27 min
21 min
Channel
29 min
22 min
33 min
24 min
41 min
25 min
Perpendicular
Parallel

Fig. 9

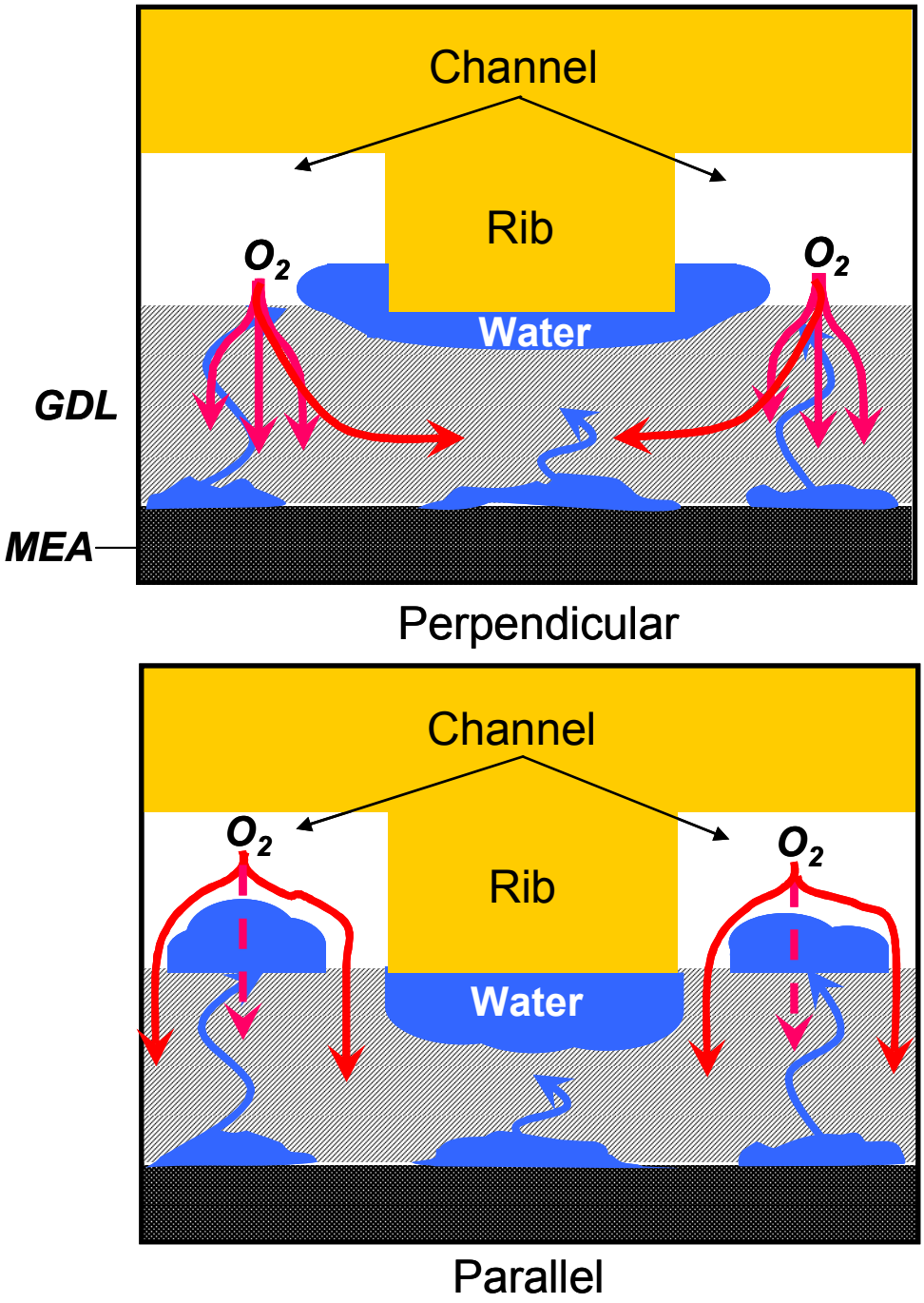
Channel
Rib
O_2
O_2
Water
GDL
MEA
Perpendicular
Channel
O_2
Rib
O_2
Water
Parallel

Fig. 10

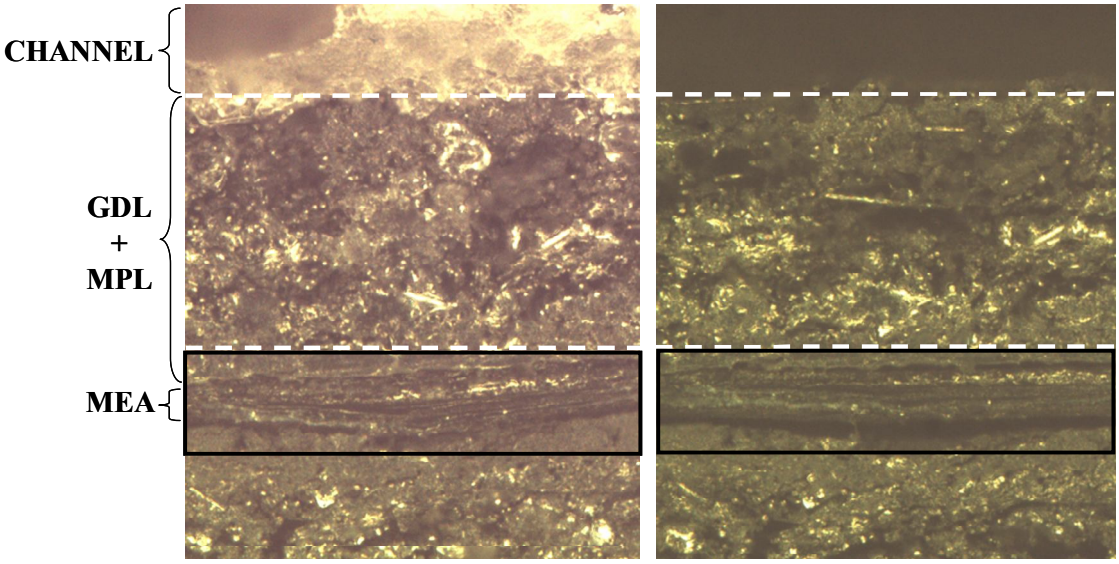

(a) Frozen photo (b) Photo after evaporated

(c) Subtracted cross-sectional photo of GDL

Fig. 11

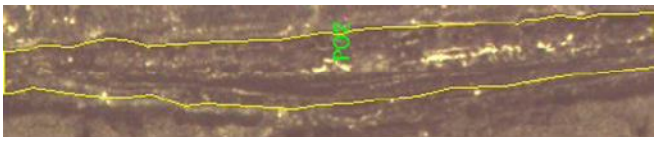

(a) Frozen state

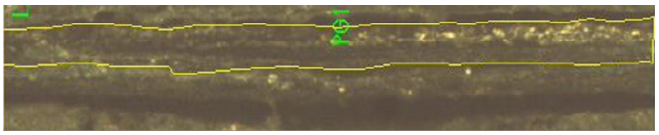

(b) Evaporated (after water removal) state

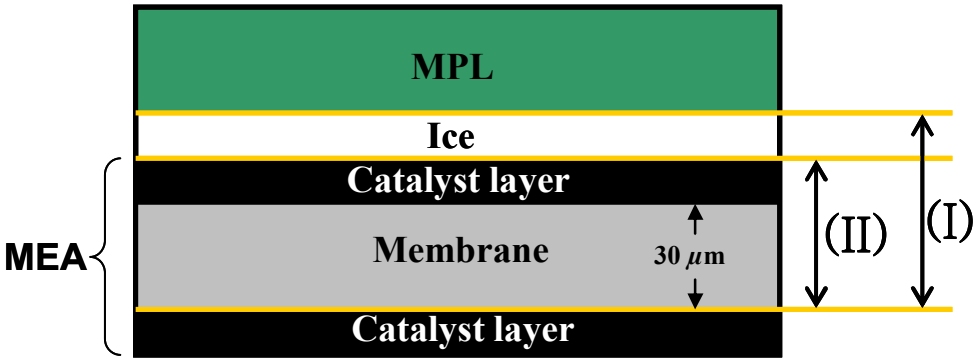

(c) Schematics diagram of MEA/MPL interface

Fig. 12

Stable condition

(Under the channel)

(Under the rib)

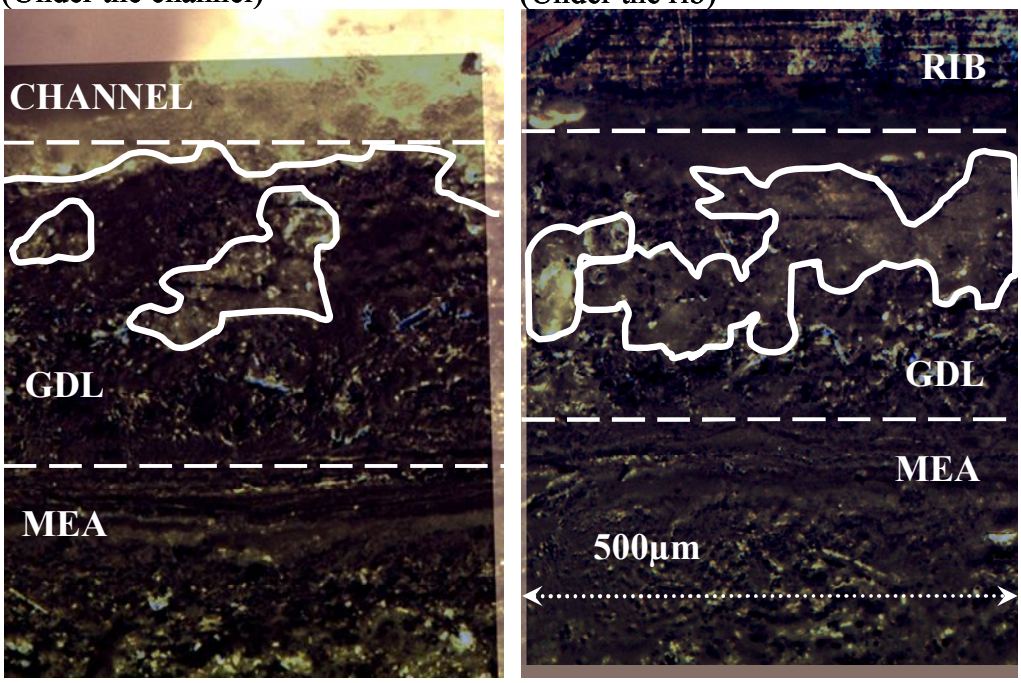

Flooded condition

(Under the channel)

(Under the rib)

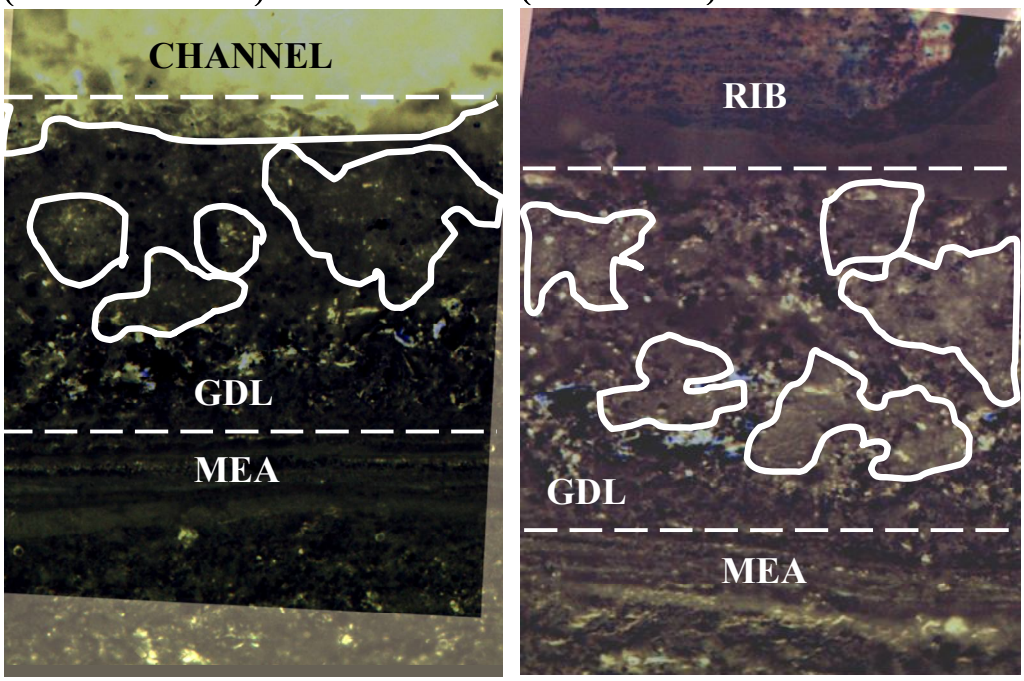

Fig. 13

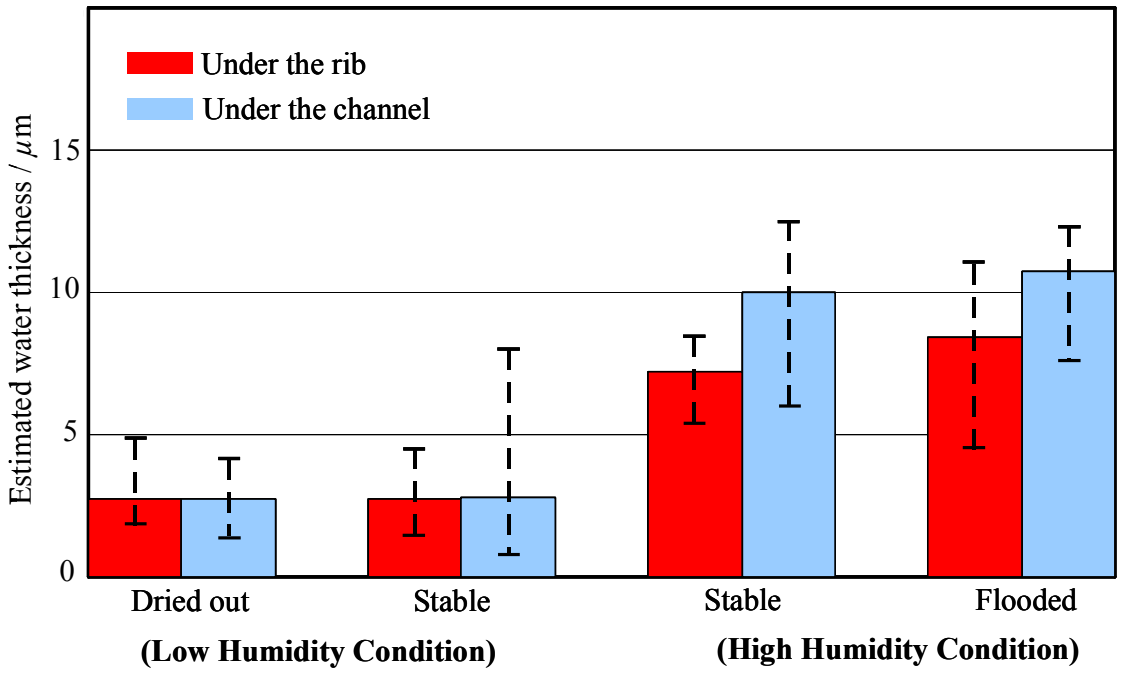
Under the rib
Under the channel
Estimated water thickness / μm
15
10
5
0
Dried out
Stable
Stable
Flooded
(Low Humidity Condition)
(High Humidity Condition)

Fig. 14

Stable condition

(Under the channel)

(Under the rib)

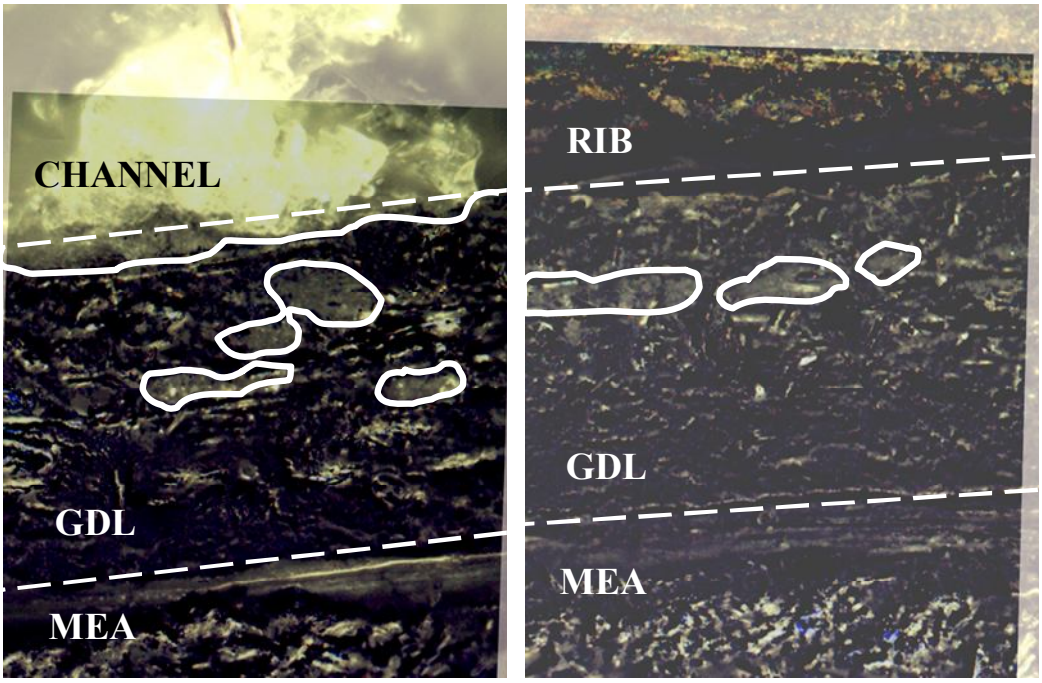

Fig. 15

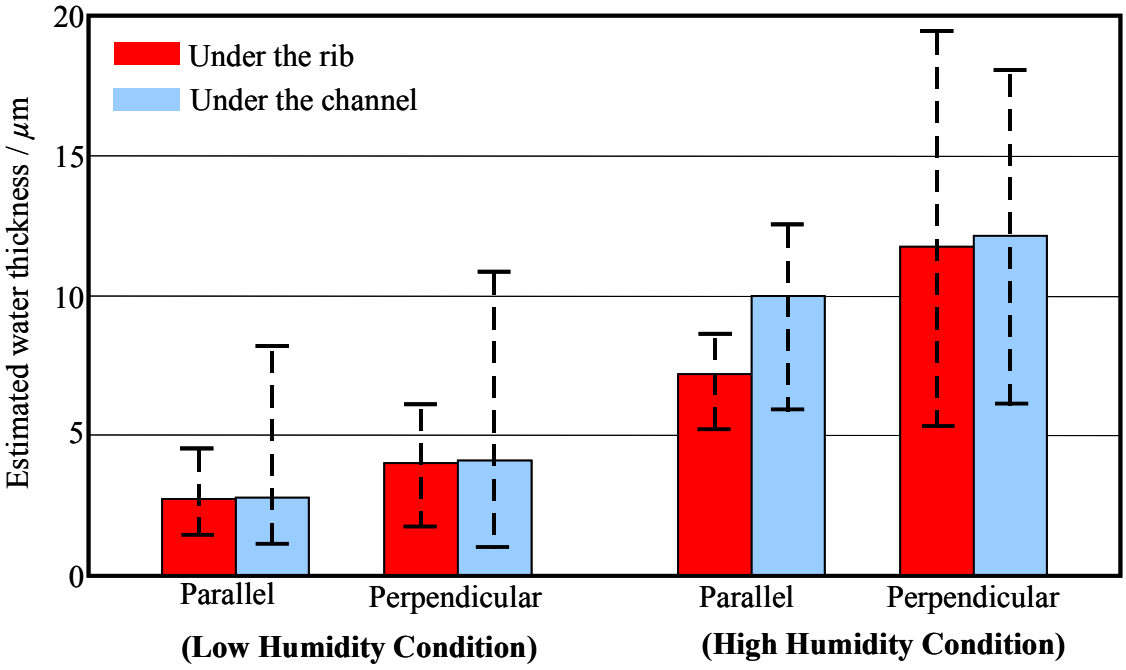
Under the rib
Under the channel
Estimated water thickness / μm
20
15
10
5
0
Parallel
Perpendicular
Parallel
Perpendicular
(Low Humidity Condition)
(High Humidity Condition)

Fig. 16

Table 1

Thickness	278 μm @0 MPa, 210 μm @2 MPa
Porosity	74%
Permeability (as Fiber direction)	0.61 x 10^{-12} $m^3Pa^{-1}sec^{-1}$ @1.8 MPa
Permeability (Transverse direction)	0.39 x 10^{-12} $m^3Pa^{-1}sec^{-1}$ @1.8 MPa
Fiber diameter	Φ12.5 μm
Maximum pore size	Φ35 μm

Table 2

No.	Channel Type	Conditions	V_{per}/V_{para}	No.	Channel Type	Conditions	V_{per}/V_{para}
1	SP.	H_2(1.25) Air(3.0) 0.5 Acm^{-2} RH90%	1.06	11	ST.	H_2(1.5) O_2(1.5) 1.0 Acm^{-2} RH90%	1.08
2	SP.	H_2(1.25) Air(3.0) 0.5 Acm^{-2} RH77%	1.08	12	ST.	H_2(2.0) O_2(2.0) 1.0 Acm^{-2} RH90%	1.10
3	SP.	H_2(1.25) Air(3.0) 0.5 Acm^{-2} RH60%	1.09	13	ST.	H_2(5.0) O_2(5.0) 1.0 Acm^{-2} RH90%	1.19
4	SP.	H_2(3.0) Air(3.0) 0.5 Acm^{-2} RH90%	1.40	14	ST.	H_2(3.0) Air(3.0) 0.5 Acm^{-2} RH70%	1.01
5	SP.	H_2(3.5) Air(3.5) 0.7 Acm^{-2} RH90%	1.22	15	ST.	H_2(5.0) Air(5.0) 0.7 Acm^{-2} RH90%	1.28
6	ST.	H_2(1.5) O_2(1.5) 0.7 Acm^{-2} RH90%	1.07	16	ST.	H_2(3.5) Air(3.5) 0.7 Acm^{-2} RH90%	1.46
7	ST.	H_2(2.0) O_2(2.0) 0.7 Acm^{-2} RH90%	1.06	17	ST.	H_2(2.0) Air(2.0) 0.7 Acm^{-2} RH90%	1.90
8	ST.	H_2(3.5) O_2(3.5) 0.7 Acm^{-2} RH90%	1.06	18	ST.	H_2(5.0) Air(5.0) 1.0 Acm^{-2} RH90%	2.14
9	ST.	H_2(5.0) O_2(5.0) 0.7 Acm^{-2} RH90%	1.06	19	ST.	H_2(3.7) Air(3.5) 0.7 Acm^{-2} RH90%	2.20
10	ST.	H_2(1.1) O_2(1.1) 1.0 Acm^{-2} RH90%	1.03				

°SP. = Serpentine Channel Separator ST. = Straight Channel Separator The values in brackets are stoichiometric ratios.